Antiferromagnetic phases of the Kondo lattice

R. Eder,[1] K. Grube,[1] and P. Wróbel[2]
[1]*Karlsruhe Institute of Technology, Institut für Festkörperphysik, D-76021 Karlsruhe, Germany*
[2]*Institute for Low Temperature and Structure Research, P.O. Box 1410, PL-50950 Wrocław 2, Poland*
(Received 4 February 2016; revised manuscript received 20 March 2016; published 7 April 2016)

We discuss the paramagnetic and Néel-ordered phases of the Kondo lattice Hamiltonian on the two-dimensional square lattice by means of bond fermions. In the doped case we find two antiferromagnetic solutions, the first one with small ordered moment, heavy bands, and an antiferromagnetically folded large Fermi surface—i.e., including the localized spins—the second one with large ordered moment, light bands, and an antiferromagnetically folded conduction electron-only Fermi surface. The zero temperature phase diagram as a function of Kondo coupling and conduction electron density shows first- and second-order transition lines between the three different phases and agrees qualitatively with previous numerical studies. We compare to experiments on $CeRh_{1-x}Co_xIn_5$ and find qualitative agreement.

DOI: 10.1103/PhysRevB.93.165111

I. INTRODUCTION

Heavy fermion compounds are a much studied class of materials in the field of strongly correlated electron systems. Among the many phenomena observed in these compounds is a variety of phase transitions between different magnetically ordered and nonmagnetic phases which occur as a function of temperature, pressure, alloying, or magnetic field. Often the transition temperature can be driven to zero Kelvin by varying some experimental parameter resulting in quantum critical points and superconductivity [1]. The simplest model believed to be able to describe these compounds is the Kondo lattice model, which is obtained from the more realistic periodic Anderson model by means of the Schrieffer-Wolff transformation [2] and describes a single conduction band coupled to a periodic array of localized spins by spin exchange,

$$H = \sum_{\mathbf{k},\sigma} \epsilon_{\mathbf{k}}\, c^{\dagger}_{\mathbf{k},\sigma} c_{\mathbf{k},\sigma} + J \sum_{i}\, \vec{S}_i \cdot \vec{\sigma}_i . \qquad (1)$$

Thereby each unit cell i is assumed to contain one conduction band (or c) orbital and one localized (or f) orbital; the operators $c^{\dagger}_{i,\sigma}$ and $f^{\dagger}_{i,\sigma}$ create an electron with z-spin σ in these. Moreover, $\vec{\sigma}_i = \frac{1}{2}\, c^{\dagger}_{i\sigma}\, \vec{\tau}_{\sigma\sigma'}\, c_{i\sigma'}$ where $\vec{\tau}$ is the vector of Pauli matrices whereas $\vec{S}_i$ denotes the spin operator of the localized electrons and $\epsilon_{\mathbf{k}}$ is the dispersion relation of the conduction band.

It is widely believed that the magnetic phase transitions are the consequence of a competition between the Kondo effect and the Ruderman-Kittel-Kasuya-Yoshida (RKKY) interaction between the localized electrons [3]. The essence of the Kondo effect is the formation of singlets between a localized electron and a conduction electron, leading to a vanishing of the expectation value $\langle \vec{S}_i \rangle$, whereas the RKKY interaction—or any other mechanism favoring magnetic order such as a magnetic field—favors a nonvanishing $\langle \vec{S}_i \rangle$. Accordingly, there is an inherent frustration in the Kondo lattice model and slight perturbations may tilt the balance and induce a phase transition. Moreover, for a lattice of localized spins the Kondo effect leads to a Fermi surface volume to which the localized electrons contribute as if they were itinerant. The transitions between "Kondo-dominated" and "RKKY-dominated" phases therefore are often accompanied by a reconstruction of the Fermi surface which goes beyond the simple generation of umklapps but rather changes the volume of the Fermi surface by an amount corresponding to half of an electron per spin and f site.

While the single impurity Kondo problem can be solved exactly the Kondo lattice Hamiltonian is less well understood. Following the work of Yoshimori and Sakurai [4], Lacroix and Cyrot [5,6] studied the Kondo lattice in mean-field theory. For a band with a constant density of states in the range $[-D : D]$ and electron densities close to $n_c = 1$ Lacroix and Cyrot found a paramagnetic and a Néel-ordered solution. At $T = 0$ the antiferromagnetic phase thereby turns out to have lower energy than the paramagnetic one for $J \leqslant D/2$. Its ordered f moment always has the maximum value of $1/2$ [5] so that the phase transition is first order. Various other mean-field studies of the Kondo lattice were performed since then [7–11] but it appears to be difficult to reproduce the phase diagrams of heavy fermion compounds by this approach.

Since then the model was also studied by renormalization group [12] and extended dynamical mean-field theory (see Ref. [13] for a recent review) and a global phase diagram was outlined [13,14]. Additional work has focused on the properties of quasiparticles near the quantum critical points [15] and the phenomenological two-fluid model was proposed (for a recent review see Ref. [16]).

In this manuscript we present an approximation in terms of bond fermions which reproduces a few results obtained previously only by numerical methods, such as the phase diagram containing two antiferromagnetic and a paramagnetic phase. As will be discussed below this phase diagram also qualitatively reproduces some experimental results on heavy fermion compounds.

II. METHOD OF CALCULATION

In the following we consider the Hamiltonian (1) on a two-dimensional (2D) square lattice of N unit cells, the number of conduction electrons is N_c and $n_c = N_c/N = 1 - \delta$. For the dispersion of the conduction band $\epsilon_{\mathbf{k}}$, we assume a

tight-binding form with hopping integrals $-t$ between nearest and t_1 between second nearest neighbors, i.e.,

$$\epsilon_{\mathbf{k}} = -2t(\cos(k_x) + \cos(k_y)) + 4t_1 \cos(k_x) \cos(k_y).$$

The calculation to be outlined below may be viewed as a fermionic version of the bond operator theory proposed by Sachdev and Bhatt to describe bosonic spin fluctuations in quantum spin systems [17] which was applied successfully to spin ladders [18]. In deriving the fermionic version we follow Ref. [19]; see also Ref. [20] for a more rigorous derivation. In the limit $t,t_1 \to 0$ and $N_c = N$ the ground state is a product of singlets,

$$|\Psi_0\rangle = \prod_{j=1}^{N} s_j^\dagger\, |0\rangle, \quad s_j^\dagger = \frac{1}{\sqrt{2}} (c_{j\uparrow}^\dagger f_{j\downarrow}^\dagger - c_{j\downarrow}^\dagger f_{j\uparrow}^\dagger). \tag{2}$$

The energy of this state is $-Ne_0$ with $e_0 = \frac{3}{4}J$. Switching on nonvanishing hopping integrals produces *charge fluctuations*, e.g., an electron with spin σ can be transferred from some cell m to another cell n, resulting in a state with three electrons in n and a single electron in m. In subsequent steps either the surplus electron or the hole may propagate to other sites or additional electron-hole pairs may be generated. In Ref. [19] the product of singlets (2) was considered as the vacuum $|\text{vac}\rangle$ for charge fluctuations which themselves were described as effective fermions (here we will call them "bond fermions") There are holelike and electronlike bond fermions, and states containing a single of these correspond to states of the true Kondo lattice as follows:

$$\begin{aligned} b_{i\sigma}^\dagger|\text{vac}\rangle &\to c_{i\uparrow}^\dagger c_{i\downarrow}^\dagger\, f_{i\sigma}^\dagger \prod_{j\neq i} s_j^\dagger\, |0\rangle, \\ a_{i\sigma}^\dagger|\text{vac}\rangle &\to f_{i\sigma}^\dagger \prod_{j\neq i} s_j^\dagger\, |0\rangle. \end{aligned} \tag{3}$$

The generalization to states with more than one bond fermion is self-evident, the only requirement being that the factors of $c_{i\uparrow}^\dagger c_{i\downarrow}^\dagger\, f_{i\sigma}^\dagger$ and $f_{j\sigma}^\dagger$ in the Kondo-lattice states be in the same order as the $b_{i\sigma}^\dagger$ and $a_{j\sigma}^\dagger$ in the bond fermion states. Since a unit cell with either one or three electrons has an exchange energy of 0 we ascribe an energy of formation of $+e_0$ to each bond fermion. Operators for the bond fermions are obtained by demanding that their matrix elements between bond fermions states be identical to those of the physical operator between the respective translated states. Due to the product nature of states like (3) this is usually easy to achieve. For example, the electron annihilation operator becomes

$$c_{i,\sigma} = \frac{1}{\sqrt{2}}(\text{sgn}(\sigma)\, a_{i,\bar\sigma}^\dagger - b_{i,\sigma}). \tag{4}$$

Fourier transformation gives the representation of $c_{\mathbf{k},\sigma}$ and inserting this into the kinetic energy $\sum_{\mathbf{k},\sigma} \epsilon_{\mathbf{k}}\, c_{\mathbf{k},\sigma}^\dagger c_{\mathbf{k},\sigma}$ the Hamiltonian becomes [19]

$$\begin{aligned} H = \sum_{\mathbf{k},\sigma} \Bigg[&\left(\frac{\epsilon_{\mathbf{k}}}{2} + e_0\right) b_{\mathbf{k},\sigma}^\dagger b_{\mathbf{k},\sigma} + \left(\frac{\epsilon_{\mathbf{k}}}{2} - e_0\right) a_{-\mathbf{k},\bar\sigma} a_{-\mathbf{k},\bar\sigma}^\dagger \\ &- \text{sgn}(\sigma)\, \frac{\epsilon_{\mathbf{k}}}{2}\, (\, b_{\mathbf{k},\sigma}^\dagger a_{-\mathbf{k},\bar\sigma}^\dagger + \text{H.c.}) \Bigg] + N\, e_0. \end{aligned} \tag{5}$$

The positive sign of the additive constant is not a misprint—rather, this is the sum of the energy of the vacuum state (2), $-Ne_0$, and a term $+2Ne_0$ obtained by inverting $2N$ products of fermion operators $e_0\, a_{-\mathbf{k},\bar\sigma}^\dagger a_{-\mathbf{k},\bar\sigma} = e_0 - e_0\, a_{-\mathbf{k},\bar\sigma} a_{-\mathbf{k},\bar\sigma}^\dagger$. In using the Hamiltonian (5) we are making two approximations: First, the possibility that a unit cell containing two electrons is in a triplet state is neglected. This means we neglect bosonic spin excitations and their coupling to the fermionic charge fluctuations. Second, states like $a_{i,\sigma}^\dagger b_{i,\sigma'}^\dagger|\text{vac}\rangle$ or $a_{i,\uparrow}^\dagger a_{i,\downarrow}^\dagger|\text{vac}\rangle$ where two bond fermions occupy the same unit cell obviously are meaningless so that the bond fermions have to obey a hard-core constraint—which we neglect in the following. This issue is discussed in detail in Sec. V.

Since the vacuum state (2) contains $2N$ electrons *including the localized electrons* and since adding an $a^\dagger$ fermion (a $b^\dagger$ fermion) decreases (increases) the electron number by one, the total number of electrons is

$$\begin{aligned} N_e &= 2N + \sum_{\mathbf{k},\sigma} b_{\mathbf{k}\sigma}^\dagger b_{\mathbf{k}\sigma} - \sum_{\mathbf{k},\sigma} a_{\mathbf{k}\sigma}^\dagger a_{\mathbf{k}\sigma} \\ &= \sum_{\mathbf{k},\sigma} (b_{\mathbf{k}\sigma}^\dagger b_{\mathbf{k}\sigma} + a_{-\mathbf{k}\bar\sigma} a_{-\mathbf{k}\bar\sigma}^\dagger). \end{aligned} \tag{6}$$

An extra complication—discussed in detail in Ref. [19]—is the following: After tuning the electron number to any prescribed value N' by adding the term $-\mu(N_e - N')$ to the Hamiltonian and adjusting μ, the $\mathbf{k}$-integrated conduction electron momentum distribution function $n_{\mathbf{k}} = \langle c_{\mathbf{k}\sigma}^\dagger c_{\mathbf{k}\sigma}\rangle$—which equals the $\mathbf{k}$- and ω-integrated photoemission weight—in general is not equal to $N_c = N' - N$. As proposed in Ref. [19] we resolve this problem by enforcing the equality of N_c and $\mathbf{k}$-integrated $n_{\mathbf{k}}$ via an additional Lagrange multiplier λ, i.e., we add the term $-\lambda(\sum_{\mathbf{k},\sigma} c_{\mathbf{k}\sigma}^\dagger c_{\mathbf{k}\sigma} - N_c)$ to H and adjust λ. This amounts to replacing $\epsilon_{\mathbf{k}} \to \epsilon_{\mathbf{k}} - \lambda$ in (5). The Hamiltonian (5) then can be solved by a unitary transformation:

$$\begin{aligned} \gamma_{\mathbf{k},1,\sigma}^\dagger &= u_{\mathbf{k}}\, b_{\mathbf{k},\sigma}^\dagger + \text{sgn}(\sigma)\, v_{\mathbf{k}}\, a_{-\mathbf{k},\bar\sigma}, \\ \gamma_{\mathbf{k},2,\sigma}^\dagger &= -\text{sgn}(\sigma)\, v_{\mathbf{k}}\, b_{\mathbf{k},\sigma}^\dagger + u_{\mathbf{k}}\, a_{-\mathbf{k},\bar\sigma}. \end{aligned}$$

In terms of the quasiparticle operators $\gamma_{\mathbf{k},\nu,\sigma}^\dagger$ the electron number (6) becomes

$$N_e = \sum_{\mathbf{k},\sigma} \sum_{\nu=1}^{2} \gamma_{\mathbf{k},\nu,\sigma}^\dagger \gamma_{\mathbf{k},\nu,\sigma}.$$

While all bond fermion basis states such as (3) have exactly one f electron per unit cell so that the f electrons are perfectly localized, the Fermi surface volume therefore is such as if the f electrons were itinerant. The quasipartile dispersion and conduction electron momentum distribution become (for $n_c \leqslant 1$)

$$\begin{aligned} E_{\mathbf{k},\pm} &= \frac{1}{2}\left((\epsilon_{\mathbf{k}} - \lambda) \pm \sqrt{(\epsilon_{\mathbf{k}} - \lambda)^2 + 4e_0^2}\right) - \mu. \\ n_{\mathbf{k}} &= \frac{1}{2}\left(1 - \frac{\epsilon_{\mathbf{k}} - \lambda}{\sqrt{(\epsilon_{\mathbf{k}} - \lambda)^2 + 4e_0^2}}\right) \Theta(\mu - E_{\mathbf{k},-}). \end{aligned}$$

For $J/t \to 0$ the band structure approaches the noninteracting $\epsilon_{\mathbf{k}}$ plus a dispersionless band at energy λ whereas $n_{\mathbf{k}} \propto \Theta(\lambda - \epsilon_{\mathbf{k}})$. In this limit both λ and μ must be set equal to

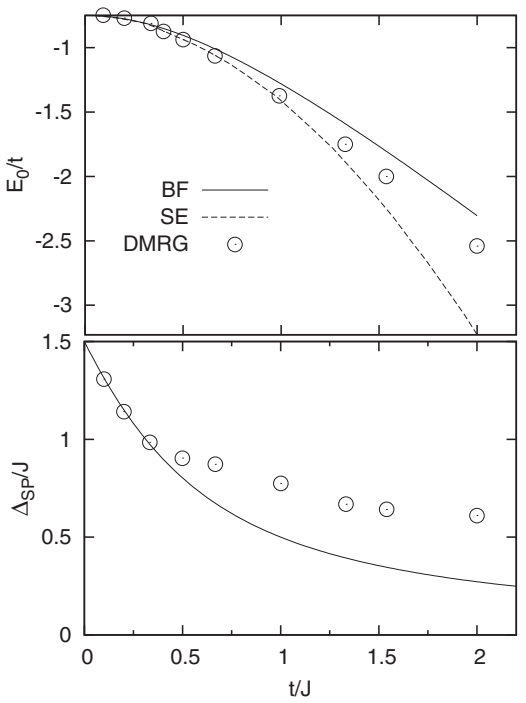

FIG. 1. Ground-state energy E_0/t per site (top) and single-particle gap $\Delta_{\rm QP}/J$ versus t/J for the 1D Kondo insulator. The line is the result from the bond fermion calculation the symbols are DMRG results by Yu and White [21]. The curve labeled SE in the top panel is the ground-state energy obtained by series expansion [22].

the noninteracting chemical potential whence the total energy becomes that of the free Fermi sea. For $J/t \to \infty$ we have two bands at $\pm e_0 + O(t)$. For $N_c < N$ the chemical potential cuts into the lower of these two bands, resulting in a total energy of $-N_c e_0 + O(t)$. Again, this is the correct limiting behavior because for $J/t \to \infty$ the ground state has N_c singlets and $N - N_c$ mobile c vacancies which contribute an energy $\propto \delta \cdot t$. The ground-state energy obtained from the bond fermion calculation accordingly interpolates between these two exactly known limiting values. Figure 1 compares some results obtained in this way for a one-dimensional (1D) chain with $n_c = 1$—i.e., the Kondo insulator—and $t_1 = 0$ to the density matrix renormalization group (DMRG) results of Yu and White [21]. Since particle-hole symmetry requires $\lambda = \mu = 0$ in this case, the bond fermion calculation gives the ground-state energy per site E_0 and single-particle gap $\Delta_{\rm SP} = E_{k=0,+} - E_{k=\pi,-}$ as

$$E_0 = e_0 - \frac{1}{\pi}\int_{-\pi}^{\pi} dk\,\sqrt{t^2\cos^2(k) + e_0^2},$$
$$\Delta_{\rm SP} = 2\left(\sqrt{e_0^2 + t^2} - t\right).$$

This agrees reasonably well with DMRG for $t/J < 1$ whereas the agreement is less satisfactory for $t/J > 1$. The panel for the energy also shows the series expansion results from Ref. [22]. The rather simple analytic bond fermion estimate is as good as the series expansion result for $t/J < 1$ but appears to be closer to the numerical result for $t/J > 1$.

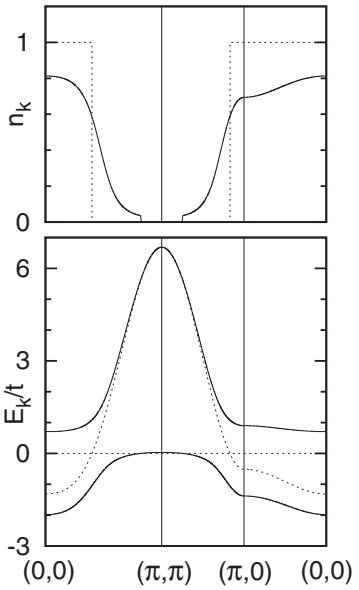

FIG. 2. Conduction electron momentum distribution (top) and band structure (bottom) for the paramagnetic phase of the 2D Kondo lattice Hamiltonian with $n_c = 0.9$, $J/t = 1.4$, and $t_1/t = 0.4$. The dashed lines show the respective quantity for noninteracting electrons.

The band structure in two dimensions for finite J/t—shown in Fig. 2—has the familiar "hybridization gap" form; $n_{\mathbf{k}}$ has a sharp but continuous drop at the noninteracting Fermi surface and a tiny discontiuity at the actual Fermi momentum. It should be stressed that since no self-consistency equation is solved in the bond fermion calculation the energy scale of the single impurity Kondo temperature, $k_B T_K = D\,\exp(1/\rho_0 J)$ (with ρ_0 the density of states at the Fermi level and D the conduction electron bandwidth) does not appear anywhere in the present calculation—if this plays a role also in the lattice case the bond fermion calculation is too crude to reproduce it.

We now generalize the calculation to a magnetically ordered phase. In (2) and (3) we replace $s_j^\dagger \to \tilde{s}_j^\dagger$ where

$$\tilde{s}_j^\dagger = \cos(\Theta)\, s_j^\dagger + e^{i\mathbf{Q}\cdot\mathbf{R}_j}\sin(\Theta)\, t_{j,z}^\dagger,$$
$$t_{j,z}^\dagger = \frac{1}{\sqrt{2}}\,(c_{j\uparrow}^\dagger f_{j\downarrow}^\dagger + c_{j\downarrow}^\dagger f_{j\uparrow}^\dagger), \qquad (7)$$

with $\mathbf{Q} = (\pi,\pi)$ the antiferromagnetic wave vector and the angle Θ will be determined subsequently by minimizing the energy. The new vacuum state may be viewed as a condensate of Bosonic z-like triplets [17,20] with momentum $\mathbf{Q}$ in the pure "singlet background" considered above and has energy $-N\tilde{e}_0$ with $\tilde{e}_0 = \frac{3J}{4}\cos^2(\Theta) - \frac{J}{4}\sin^2(\Theta)$. For $\Theta = 0$ we recover the original paramagnetic vacuum state whereas for $\Theta = \frac{\pi}{4}$ we have the fully polarized Néel state with the opposite ordered moment for c and f electrons. The energy of a bond fermion now is $\tilde{e}_0$ and instead of (4) we find

$$c_{i,\uparrow} = a_+ a_{i,\downarrow}^\dagger - a_- b_{i,\uparrow},$$
$$c_{i,\downarrow} = -a_- a_{i,\uparrow}^\dagger - a_+ b_{i,\downarrow},$$
$$a_\pm = \frac{\cos(\Theta) \pm e^{i\mathbf{Q}\cdot\mathbf{R}_i}\sin(\Theta)}{\sqrt{2}}.$$

We introduce the sublattices A and B whereby A contains (0,0) and accordingly introduce two species of bond Fermions, e.g., $b^\dagger_{i,\sigma}$ for $i \in A$ and $\tilde{b}^\dagger_{j,\sigma}$ for $j \in B$ (and analogously for the $a^\dagger$'s). The Fourier transforms of the electron operators are

$$
\begin{aligned}
c_{\mathbf{k},\uparrow} &= -c_- b_{\mathbf{k},\uparrow} - c_+ \tilde{b}_{\mathbf{k},\uparrow} + c_- \tilde{a}^\dagger_{-\mathbf{k},\downarrow}, + c_+ a^\dagger_{-\mathbf{k},\downarrow},\\
c_{\mathbf{k}+\mathbf{Q},\uparrow} &= -c_- b_{\mathbf{k},\uparrow} + c_+ \tilde{b}_{\mathbf{k},\uparrow} - c_- \tilde{a}^\dagger_{-\mathbf{k},\downarrow}, + c_+ a^\dagger_{-\mathbf{k},\downarrow},\\
c_{\mathbf{k},\downarrow} &= -c_+ b_{\mathbf{k},\downarrow} - c_- \tilde{b}_{\mathbf{k},\downarrow} - c_+ \tilde{a}^\dagger_{-\mathbf{k},\uparrow}, - c_- a^\dagger_{-\mathbf{k},\uparrow},\\
c_{\mathbf{k}+\mathbf{Q},\downarrow} &= -c_+ b_{\mathbf{k},\downarrow} + c_- \tilde{b}_{\mathbf{k},\downarrow} + c_+ \tilde{a}^\dagger_{-\mathbf{k},\uparrow}, - c_- a^\dagger_{-\mathbf{k},\uparrow},\\
c_\pm &= \tfrac{1}{2}(\cos(\Theta) \pm \sin(\Theta)),
\end{aligned}
$$

where $\mathbf{k}$ denotes a wave vector in the antiferromagnetic brillouin zone (AFBZ). By again inserting the above representations of $c_{\mathbf{k},\sigma}$ into the kinetic energy we obtain the Hamiltonian. Introducing the column vector, $\mathbf{v}_\sigma(\mathbf{k}) = (b_{\mathbf{k},\sigma}, \tilde{b}_{\mathbf{k},\sigma}, \tilde{a}^\dagger_{-\mathbf{k},\bar{\sigma}}, a^\dagger_{-\mathbf{k},\bar{\sigma}})^T$ H becomes

$$
\begin{aligned}
H &= \sum_{\mathbf{k}\in AFBZ} \sum_\sigma \mathbf{v}^\dagger_\sigma(\mathbf{k})\, H_\sigma(\mathbf{k})\, \mathbf{v}_\sigma(\mathbf{k}) + N\, \tilde{e}_0,\\
H_\sigma(\mathbf{k}) &= H_J + (\epsilon^{(+)}_{\mathbf{k}} - \lambda)\, W^{(+)}_\sigma + \epsilon^{(-)}_{\mathbf{k}}\, W^{(-)}_\sigma,\\
H_J &= \mathrm{diag}(\tilde{e}_0, \tilde{e}_0, -\tilde{e}_0, -\tilde{e}_0),\\
\epsilon^{(\pm)}_{\mathbf{k}} &= \frac{1}{2}(\epsilon_{\mathbf{k}} \pm \epsilon_{\mathbf{k}+\mathbf{Q}}),
\end{aligned}
$$

and the matrices W are given by

$$
W^{(+)}_\sigma = \begin{pmatrix} \alpha_\mp, & 0, & 0, & \mp\beta \\ 0, & \alpha_\pm, & \mp\beta, & 0 \\ 0, & \mp\beta, & \alpha_\mp, & 0 \\ \mp\beta, & 0, & 0, & \alpha_\pm \end{pmatrix},
$$

$$
W^{(-)}_\sigma = \begin{pmatrix} 0, & \beta, & \mp\alpha_\mp, & 0 \\ \beta, & 0, & 0, & \mp\alpha_\pm \\ \mp\alpha_\mp, & 0, & 0, & \beta \\ 0, & \mp\alpha_\pm, & \beta, & 0 \end{pmatrix}.
$$

Here the upper (lower) sign on the respective right-hand side refers to $\sigma = \uparrow$ ($\sigma = \downarrow$) and $\alpha_\pm = \frac{1}{2}(1 \pm \sin(2\Theta))$ and $\beta = \frac{1}{2}\cos(2\Theta)$. The number of electrons is

$$
N_e = \sum_{\mathbf{k}\in AFBZ} \sum_\sigma \sum_{\nu=1}^{4} \gamma^\dagger_{\mathbf{k},\nu,\sigma} \gamma_{\mathbf{k},\nu,\sigma}.
$$

Again, the electron number is obtained by filling the four bands as if the f electrons were itinerant and did participate in the Fermi surface volume and the value of $\langle N_e \rangle$ is fixed by tuning the chemical potential μ. The parameter λ is again adjusted to match real-space count and $\mathbf{k}$-space count for the conduction electrons, i.e.,

$$
\sum_{\mathbf{k}\in AFBZ} \langle n_{\mathbf{k}} + n_{\mathbf{k}+\mathbf{Q}} \rangle = N_e - N,
$$

whereby

$$
n_{\mathbf{k}} + n_{\mathbf{k}+\mathbf{Q}} = \sum_\sigma \mathbf{v}^\dagger_\sigma\, W^{(+)}_\sigma\, \mathbf{v}_\sigma.
$$

In this way, the energy $\langle H \rangle$ can be calculated as a function of the angle Θ and minimized with respect to Θ.

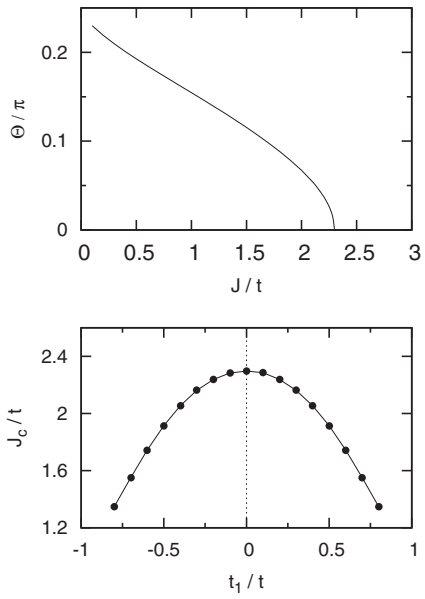

FIG. 3. (Top) Optimal angle Θ at $n_c = 1$ and $t_1/t = 0$ versus J/t. (Bottom) Values of J_c/t where the phase transition occurs as a function of t_1/t.

III. RESULTS

Figure 3 shows the angle Θ which minimizes the energy as a function of the ratio J/t for $n_c = 1$ (i.e., the so-called Kondo insulator) and $t_1 = 0$. At a certain $J_c \approx 2.29\, t$ Θ starts to deviate from the value $\Theta = 0$ which gives optimum energy at large J/t, signaling a continuous—i.e., second-order—phase transition to a magnetically ordered state (in the following J_c will always denote the value of J below which antiferromagnetism sets in for the Kondo insulator). For $J/t \to 0$ $\Theta \to \frac{\pi}{4}$, which means that the ordered f moment approaches its maximum. Figure 3 also shows the value of J_c/t obtained for different values of t_1/t. Switching on t_1 reduces J_c/t whereby to good accuracy $J_c/t = 2.29 - 1.50\,(t_1/t)^2$. This illustrates the change of the RKKY interaction due to the deformation of the Fermi surface.

The exact value of $J_c/t = 1.45$ for the case $t_1 = 0$ has been obtained by Assaad by quantum Monte Carlo (QMC) calculation [23]. The bond fermion value is larger by a factor of 1.6 which is on one hand somewhat disappointing but on the other hand the energy difference between the paramagnetic and antiferromagnetic phase is quite small—see below—so that some deviation is to be expected. Figure 4 compares the ordered moment,

$$
m_\alpha = \frac{1}{2N} \sum_i e^{i\mathbf{Q}\cdot\mathbf{R}_i} \langle n^\alpha_{i,\uparrow} - n^\alpha_{i,\downarrow} \rangle,
$$

with $\alpha \in \{c, f\}$ and the quasiparticle gap Δ_{QP} obtained from the bond fermion formalism and QMC [23]. Here we define Δ_{QP} as the energy between the highest occupied and lowest unoccupied values of $E_{\nu,\mathbf{k}}$ so that the numerical values should be twice the ones given in Ref. [23]. When plotted versus J/J_c the ordered moment agrees reasonably well with the QMC results. In the QMC calculation the ordered moment is obtained as the square root of the static structure factor so that

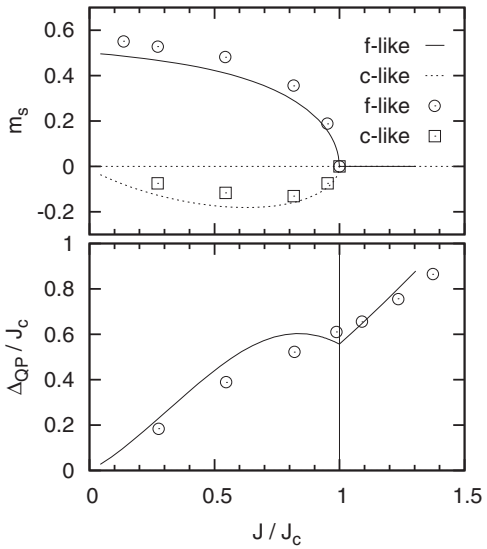

FIG. 4. (Top) Ordered moment from the bond fermion calculation (lines) versus J/J_c compared to QMC (symbols) [23]. (Bottom) Single-particle gap Δ_{QP} from the bond fermion calculation (line) versus J/J_c compared to QMC (symbols) [23].

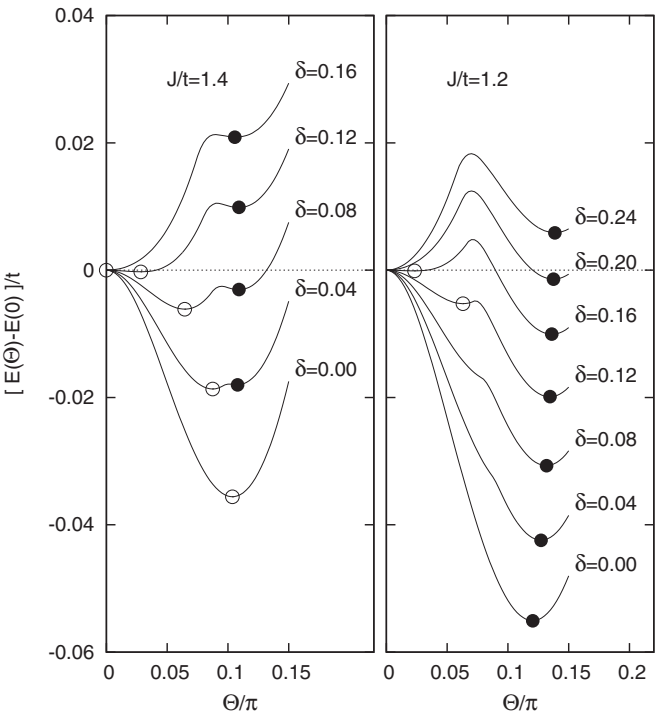

FIG. 5. Ground-state energy versus Θ for different δ and $t_1/t = 0.4$.

its sign is undetermined. The bond fermion calculation predicts the f and c ordered moments to have the opposite sign—which appears plausible due to their antiferromagnetic coupling—and we have assumed this to be true also for the QMC results. From their dynamical mean-field theory calculations Peters and Pruschke indeed found the opposite direction of m_c and m_f in Ref. [24]. The ordered moment of the f electrons approaches the maximum value of 0.5 as $J/t \to 0$ whereas the c-electron ordered moment approaches zero as $J/t \to 0$. This is to be expected because the c moment is reduced by charge fluctuations and as $J \to 0$ the effective staggered field due to the ordered f spins vanishes. The quasiparticle gap agrees reasonably well with the QMC result and is roughly linear in J. In the bond fermion result there is a kink at $J = J_c$ which is not present in the QMC data. On the other hand, using the dynamical cluster approximation Martin *et al.* indeed found a very similar kink in the Δ_{QP}-versus-J curve [25]. We proceed to the doped case. Figure 5 shows the energy as a function of Θ for different δ whereby $t_1/t = 0.4$, and $J/t = 1.4$ or $J/t = 1.2$. As δ increases there appears—in addition to the minimum for the Kondo insulator—a "wiggle" in the E vs Θ curves which develops into a second minimum. For $J/t = 1.4$ the lower of the two minima shifts to smaller Θ with increasing δ and merges with the maximum at $\Theta = 0$ into a new minimum at this angle. This corresponds to a hole-doping driven second-order transition from the antiferromagnetic to the paramagnetic phase. The second minimum—which always is higher in energy and thus never realized—moves to slightly larger Θ and crosses above the extremum at $\Theta = 0$ well before the second-order transition occurs.

This behavior changes for the value $J/t = 1.2$. The minimum for the Kondo insulator now shifts to larger values of Θ as δ increases and crosses above the extremum at $\Theta = 0$ between $\delta = 0.20$ and $\delta = 0.24$—which corresponds to a first-order transition. The second minimum still undergoes the second-order transition but now is always higher in energy and thus never realized. We therefore have two antiferromagnetic phases with different behavior upon increasing doping. In the following we refer to the phase undergoing the second-order transition as AF I, the other one as AF II.

It is also apparent from Fig. 5 that the energy difference between the antiferromagnetic and paramagnetic phases at $\delta = 0$ is only $\approx 0.05\,t$ per site. The energy per site of the paramagnetic phase itself at $\delta = 0$ and $J/t = 1.4$ is $-1.82\,t$ so that the energy difference between the two phases is only a few percent of this value despite the fact that the value of J/t is already far below J_c/t. Obviously the relatively simple bond fermion calculation does not reach such a level of accuracy so that the value of J_c/t is off by a factor of 1.6.

Proceeding as above we can map out the phase diagram in the $J - \delta$ plane which is shown in Fig. 6 for the two values $t_1/t = 0.4$ and $t_1/t = 0.0$. The line separating the AF I and paramagnetic phase corresponds to a second-order transition; the line separating the AF II from either the AF I or the paramagnetic phase represents a first-order transition. The coexistence curves between AF I and AF II do not reach the $\delta = 0$ axis because for very small doping there is only a single minimum in the energy-versus-Θ curves; see Fig. 5.

Figure 7 compares the phase diagram to that obtained by Watanabe and Ogata [26] using the variational Monte Carlo (VMC) method. For $t_1 = 0$, VMC finds $J_c/t = 1.7$, close to the exact result $J_c/t = 1.45$ from QMC [23]. When plotting the phase diagram as a function of J/J_c and δ as in Fig. 7 the bond fermion result agrees reasonably well with the VMC phase diagram. As will be discussed below, the nature of the AF I and AF II phases also agrees with VMC. A qualitatively similar phase diagram has also been obtained by Lanata

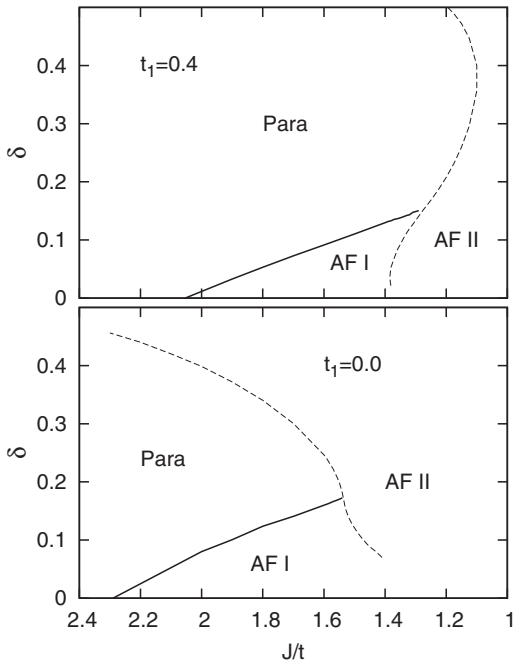

FIG. 6. Phase diagram of the Kondo lattice on a 2D square lattice as a function of Kondo coupling J and hole density δ.

et al. using the Gutzwiller approximation in Ref. [27] and by Asadzadeh *et al.* also by using the VMC method [11].

To understand the nature of the two antiferromagnetic phases Fig. 8 shows their band structure and momentum distribution function whereas Fig. 9 shows the Fermi contours in the brillouin zone. For AF I the band structure may be thought of as having been obtained from the paramagnetic one in Fig. 2 by antiferromagnetic folding plus the formation of

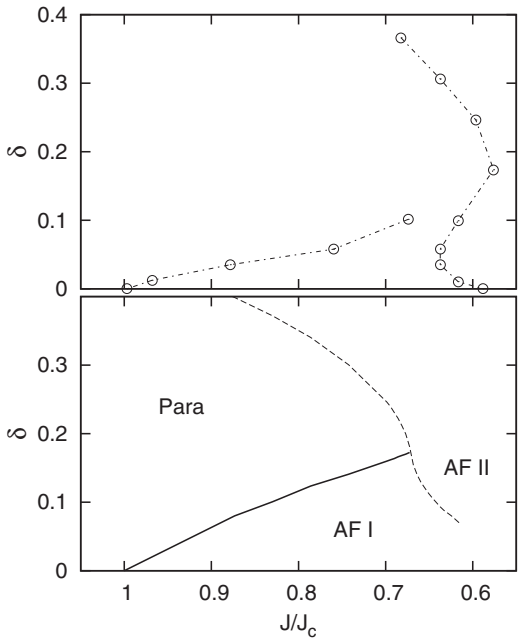

FIG. 7. Phase diagram for $t_1/t = 0$ obtained by VMC [26] (top) compared to the phase diagram from bond fermion theory (bottom).

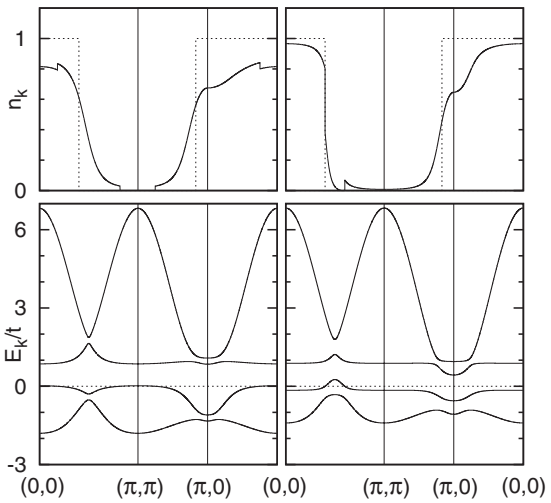

FIG. 8. (Top) Momentum distribution (top) and band structure (bottom) for the AF-I phase (left) and AF-II phase (right). In both panels $t_1/t = 0.4$, $\delta = 0.1$ whereas $J/t = 1.4$ for the AF-I phase and $J/t = 1.2$ for AF-II.

small "antiferromagnetic gaps" at the intersection points of the original and folded bands. Accordingly the Fermi surface is a hole pocket around (π,π) plus its antiferromagnetic umklapp around (0,0). As can be seen from the tiny discontinuities in $n_{\mathbf{k}}$ and the small slope of the bands, the "heavy part" of the paramagnetic band persists in this phase but undergoes antiferromagnetic folding. This is quite different for AF II. There is still a dispersionless band close to E_F but the Fermi surface is now formed by a more strongly dispersive band which has a strong c character. The Fermi surface now consists of a small pocket around $(\frac{\pi}{2},\frac{\pi}{2})$ which may be thought of as having being obtained by hybridizing the conduction electron Fermi surface for electron density $n_c = 0.9$ and its antiferromagnetic umklapp (for $t_1 = 0$ the Fermi surface in the AF-II phase really is identical to the noninteracting conduction

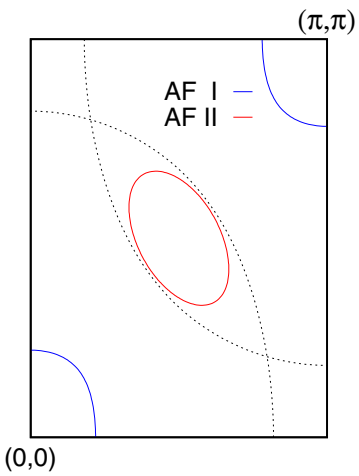

FIG. 9. The Fermi surface for the two antiferromagnetic phases in Fig. 8. The dashed lines are the noninteracting Fermi surface and its antiferromagnetic umklapp.

electron Fermi surface plus its umklapp because in this case there is no overlap between the original Fermi surface and umklapp). The discontinuity in $n_{\mathbf{k}}$ is much larger than for the AF I solution at the side of the pocket facing (0,0) whereas it is small at the part of the pocket facing (π,π) (as is also familiar from the spin-density wave mean-field solution to the Hubbard model). The plot of $n_{\mathbf{k}}$ also shows why the AF II phase is favored for small J/t: The expectation value of the kinetic energy can be written as $\langle H_t \rangle = 2\sum_{\mathbf{k}} \epsilon_{\mathbf{k}}\, n_{\mathbf{k}}$ and this is minimized by the noninteracting function $n_{\mathbf{k}}^{(0)} = \Theta(\mu - \epsilon_{\mathbf{k}})$. Figure 8 shows that the phase AF II has an $n_{\mathbf{k}}$ which is closer to the noninteracting one and thus has a lower kinetic energy than both the paramagnetic and the AF I phase.

A very similar classification of the AF I and AF II phase has been given by Watanabe and Ogata [26] based on their VMC calculations. On the other hand, a quite different phase diagram was obtained by Martin and Assaad using the dynamical cluster approximation (DCA) [28]. This authors find only one antiferromagnetic phase with a Fermi surface which does not include the f electrons—which would corresponding to the AF II solution above. Interestingly, the band structure shown in Fig. 5 of Ref. [28] also has some similarity with that of the AF II phase in Fig. 8. Martin and Assaad find that the ordered moment vanishes continuously at the phase transition between the antiferromagnetic and paramagnetic phases suggesting it to be second order despite the discontinuous change of the Fermi surface. Upon adding a nonvanishing t_1 the DCA does give also a phase corresponding to the AF-I phase, but the obtained phase diagram is quite different [25]. Figure 10 shows the development of some quantities for fixed $\delta = 0.08$ upon variation of J/t from $J/t = 1.2$ and $J/t = 1.8$. The value $t_1/t = 0.4$ so that one should compare to the upper panel of Fig. 6. At $J/t \approx 1.36$ the energies of the AF-I and AF-II phases cross resulting in a first-order phase transition. The ordered f moment drops by roughly $1/3$ at the transition, whereas the density of states at the Fermi level—which is proportional to the effective mass—increases significantly. At $J/t \approx 1.64$ the ordered moment vanishes continuously at the second-order transition and the density of states at the Fermi level smoothly approaches that of the paramagnetic phase. Similar behavior has been found by Lanata *et al.* using a Gutzwiller wave function [27] and more recently by Kubo using VMC for the periodic Anderson lattice [29].

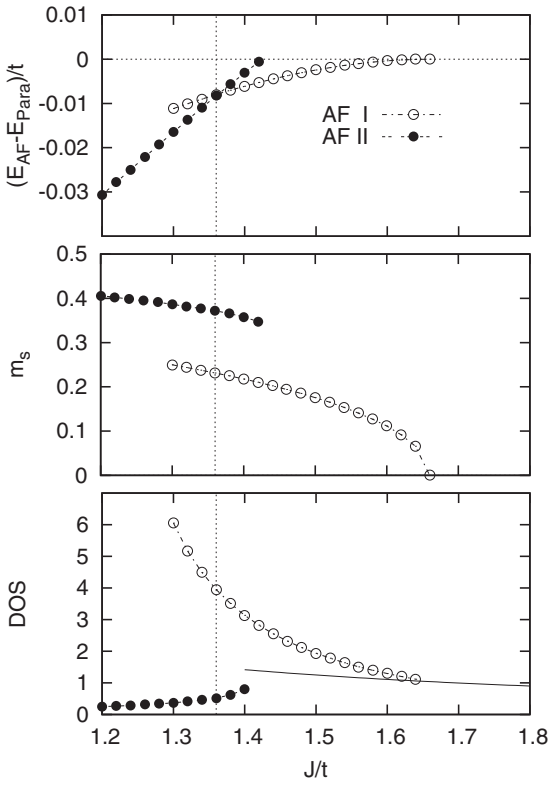

FIG. 10. Ground-state energy relative to the paramagnetic phase, ordered f-like moment m_s, and density of states per lattice site, spin, and energy t at the Fermi level (DOS) as a function of J/t for $\delta = 0.08$ and $t_1/t = 0.4$. All data are shown for the AF-I and AF-II phases; the phase transition at $J/t = 1.36$ is marked by the dashed vertical line. The full line in the panel for DOS is the density of states for the paramagnetic solution.

IV. COMPARISON TO EXPERIMENT

Let us next discuss the possible relevance of these results for experiments on $4f$-electron compounds. Here especially the compounds $CeCoIn_5$, $CeRhIn_5$, and $CeIrIn_5$ come to mind. These have a layered tetragonal crystal structure where CeIn planes parallel to the a-b plane and—say—$CoIn_4$ double layers are stacked alternatingly along the c axis [30]. The Ce ions in the CeIn planes form a 2D square lattice as considered in the present calculation.

$CeRhIn_5$ is antiferromagnetic and the ordered moment within a given CeIn plane forms the simple two-sublattice Néel order assumed in the present calculation. More precisely, there are several antiferromagnetic phases all of which have simple Néel order within the CeIn planes, but differ in the component of the magnetic ordering vector perpendicular to these. The Fermi surface of $CeRhIn_5$ as measured by de Haas-van Alphen experiments appears to consist of several roughly cylindrical and quasi-2D sheets; the measured cross sections at ambient pressure are very similar to those of $LaRhIn_5$ [30] which implies that the Ce-4f electrons do not contribute to the Fermi surface volume. Pure $CeRhIn_5$ at ambient pressure would thus correspond to the AF II phase discussed above (the magnetic order is actually incommensurate in the c direction but this is too subtle a detail for our highly simplified model anyway). In contrast, the volume of the Fermi surfaces of $CeCoIn_5$ and $CeIrIn_5$ is consistent with itinerant Ce-4f electrons [30]. The Fermi surface volume and magnetic structure $CeRhIn_5$ can be changed by either applying pressure or by substituting Rh by Co or Ir. Thereby a reduction of the lattice constant by either applying pressure or by substituting Rh ions by the isovalent but smaller Co ions in the alloy $CeRh_{1-x}Co_xIn_5$ have a different effect.

Alloying with Co in $CeRh_{1-x}Co_xIn_5$ first—at $x \approx 0.4$—induces a phase transition between two antiferromagnetic phases, from the incommensurate antiferromagnetic (ICAM) phase with an incommensurate c component of the ordering vector to the commensurate antiferromagnetic (CAM) phase with strict three-dimensional (3D) Néel order [31]. The Fermi surface volume changes from $CeRhIn_5$-like in the ICAM phase

to $CeCoIn_5$-like in the CAM phase so that the transition from localized to itinerant Ce-4f electrons occurs at this transition between the two antiferromagnetic phases and not at the transition to the paramagnetic phase [31]. The ordered moment drops from 0.38 μ_B/Ce in the ICAM phase to 0.21 μ_B/Ce in the CAM phase [32]; the cylotron mass increases from $4m_0$ to $10m_0$ [31]. It was moreover found that the Néel temperature is discontinuous across this transition which suggests it to be first order [33]. Increasing the doping to $x \approx 0.85$ induces a second phase transition to the paramagnetic phase whereby neither the Fermi surface volume nor the cyclotron mass show any discontinuity [31].

Identifying the ICAM phase with the AF II phase and the CAM phase with the AF I phase and assuming that alloying with Co simply amounts to increasing J/t due to the contraction of the lattice at constant n_c, all of this would qualitatively match the behavior in Fig. 10 quite well: a first-order transition from the AF II phase with large moment, light effective mass, and a Fermi surface which comprises only the c electrons to the AF I phase with small ordered moment, large effective mass, and a Fermi surface which comprises both c and f electrons, followed by a second-order transition to the paramagnetic phase where neither the effective mass nor the Fermi surface volume change. That the component of the ordering vector perpendicular to the CeIn planes changes at the transition between the AF II and AF I phases would not be too surprising. If the hopping matrix elements in the c direction change with the component of the Bloch wave vector $\mathbf{k}$ within the CeIn plane, $t_z = t_z(k_x,k_y)$, a relatively strong change of the Fermi contour as in Fig. 9 certainly can strongly modify the coupling between the planes and thus affect the ordering vector.

On the other hand, applying pressure to $CeRhIn_5$ leads to a completely different behavior. At $\approx 1\,GPa$ there is a first transition—or rather a "crossover"—where only the component of the magnetic ordering vector perpendicular to the CeIn planes changes [34]. No change of either the Fermi surface volume or the cyclotron mass is observed at this crossover [35]. In our simplified model a change of the magnetic order perpendicular to the planes cannot be modeled so we ignore this transition. One possible explanation for this transition would be that the effective mass changes with pressure—as seen in Fig. 10 if one assumes that pressure changes J/t—and if the interplane hopping t_z is renormalized by the quasiparticle weight $Z \propto m_{\mathrm{eff}}^{-1}$ [36] this may as well influence the coupling between planes. Increasing the pressure further induces a second transition at $p_0 = 2.3\,GPa$ to a paramagnetic phase whose Fermi surface cross sections are identical to those of $CeCoIn_5$—corresponding to itinerant Ce-4f electrons—whereas the cyclotron masses seem to diverge at the transition [35]. The limiting values of the cyclotron masses approached for large $|p - p_0|$ on the two sides of the transition differ considerably, whereby the values in the paramagnetic phase are larger by a factor of ≈ 4. With the exception of the divergence of the cyclotron mass at the transition—which cannot be reproduced by a simple theory as the present one—this could correspond to a direct (first-order) transition AF-II $\rightarrow$ Para in the phase diagram in Fig. 6.

Generally, reducing the volume of the lattice by either applying pressure or isovalent doping with ions with a smaller ionic radius may be expected to enhance the overlap of atomic orbitals so that all hopping elements increase, but the rate of increase varies with the character of the two connected orbitals. On the other hand, the intraatomic Coulomb repulsion U will remain essentially unchanged, whereas the charge transfer energy ϵ_f may change due to a variation of the Madelung potential although it is hard to predict if ϵ_f increases or decreases. From the Schrieffer-Wolff transformation the Kondo exchange constant $J = 2V^2((U+\epsilon_f)^{-1} + \epsilon_f^{-1})$ where V is the $c-f$ hybridization. Due to the higher power of V in J, a plausible guess is that J/t increases upon contraction of the crystal. On the other hand, this may not be the only effect of the contraction. Since the hybridization integrals between different pairs of orbitals change at a different rate, the width of different bands also may change at a different rate. Accordingly it may happen that small "uncorrelated" electron or hole pockets participating in the Fermi surface—which are known to exist in $CeRhIn_5$ from de-Haas van-Alphen experiments [30,35]—may shrink or expand if the band which forms the pocket changes its width at a different rate as compared to the band which mixes with the 4f electrons. In this way, electrons may be transferred from the pockets to the band which interacts with the localized moments or vice versa so that contraction of the lattice may in addition change also the conduction electron density n_c in our simplified model. Having noticed this we conclude that it may also make a difference if the contraction is due to hydrostatic pressure or by doping the material with ions that have a smaller ionic radius because these perturbations may affect different bonds in the solid in a different way. Therefore it might not be too surprising if applying hydrostatic pressure or alloying with Co would drive $CeRhIn_5$ through a phase diagram like that in Fig. 6 along different routes.

Another example for a compound undergoing a pressure-induced phase transition from an antiferromagnetic phase to a paramagnetic phase is $CeRh_2Si_2$ [37] which also has layered structure comprising planes where Ce atoms form a 2D square lattice. At $p_0 = 1.1\,GPa$ antiferromagnetism disappears and the Fermi surface changes from being consistent with the density functional Fermi surface of $LaRh_2Si_2$ to being consistent with that for $CeRh_2Si_2$—which again corresponds to the Ce-4f electrons changing from localized to itinerant [37]. Whereas three sheets of the Fermi surface could be resolved at ambient pressure only one sheet is observed above p_0 and this has a cyclotron mass which is larger by a factor of 2–4 than the ones below p_0. Again, there seems to be a transition from an antiferromagnetic phase with localized f electrons and relatively light masses to a paramagnetic phase with itinerant f electrons and heavy masses which might correspond to the transition AF II $\rightarrow$ paramagnetic in the calculated phase diagram. Lastly, a transition between two different antiferromagnetic phases has been observed in $CeCu_{6-x}Au_x$ [38]. Applying pressure to $CeCu_{5.5}Au_{0.5}$ results in an apparent first-order transition between two phases which differ in their ordering vector.

V. ON THE VIOLATION OF THE CONSTRAINT

Lastly we discuss the approximations that were made. As already stated, the bond fermions in principle have to obey a

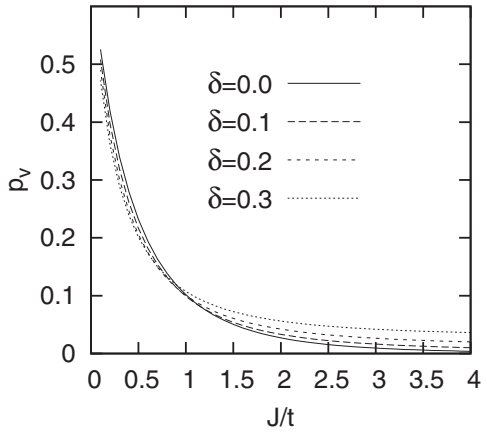

FIG. 11. Probability p_v for violation of the constraint in the paramagnetic solution versus J/t for different hole doping δ.

hard-core constraint, that means no two of them—which could differ either in their spin or species—are allowed to occupy the same unit cell because such a state cannot be translated meaningfully to a state of the true Kondo lattice. Instead, in all the above calculations the bond fermions were treated as free fermions which is an uncontrolled approximation. However, there is a simple way to judge how much this assumption is justified, namely to calculate for the ground state so obtained the probability p_v that the constraint is violated at a given site. Since we are dealing with noninteracting fermions this is easily evaluated. There are five allowed states of a given cell, namely the empty cell or a state with a single bond fermion of either spin direction and either species. The probability for the cell to be in one of these five allowed states is

$$p_a = (1-n_a)^2\,(1-n_b)^2 + 2n_a\,(1-n_a)\,(1-n_b)^2 + 2n_b\,(1-n_a)^2\,(1-n_b),$$

where $n_a = \langle\, a^\dagger_{i,\sigma} a_{i,\sigma}\,\rangle$ and similar for n_b. The probability for the constraint to be violated then is $p_v = 1 - p_a$. Figure 11 shows p_v as a function of J/t for different dopings. For values of $J/t > 1$ one has $p_v \leqslant 0.1$.

To put this in perspective, we consider other cases where a constraint is relaxed. In linear spin wave theory for the spin-$\frac{1}{2}$ Heisenberg antiferromagnet [39] the Bosonic magnons have to obey a hard-core constraint because a given spin can be flipped only once relative to the Néel order so that the presence of two magnons at the same site is unphysical. From the known reduction of the ordered moment one can infer that even for the 2D case—where quantum fluctuations are strongest—the density of magnons is only $n_b = 0.197$ per site. Accordingly, the probability that two magnons occupy the same site—and thus violate the constraint—is $p_v \approx n_b^2 = 0.04$. In fact, linear spin wave theory gives an excellent quantitative description of Heisenberg antiferromagnets.

As a second example we consider mean-field theories for the Kondo lattice [5–8]. There the Heisenberg exchange is Hartree-Fock decoupled resulting in a mean-field Hamiltonian which is a quadratic form and describes the mixing between the original conduction band and a dispersionless band of f electrons. The number of f electrons then is adjusted to one per unit cell by tuning the energy of the effective f level. Since the f electrons are uncorrelated and their density is 0.5 per unit cell and spin, the probability that there are either 2 or 0 f electrons in a cell so that the constraint is violated is $p_v = 0.5$

For the bond Fermions the probability for a violation of the constraint thus is not as small as in linear spin wave theory and one may expect stronger deviations, e.g., for the ground-state energy which probably is the reason for the incorrect value of J_c/t.

One might consider an approximate treatment of the hard-core constraint by Gutzwiller projection or by a mean-field theory similar to the one proposed by Sachdev and Bhatt [17]. In fact, using the mean-field procedure for the Kondo insulator with $t_1 = 0$ Jurecka and Brenig obtained the value $J_c/t = 1.5$, very close to the exact value from QMC [20]. However, we have tried both methods and abandoned them because both of them lead to a substantial narrowing of the conduction band. On the other hand, all available numerical results for the single-particle spectral function of the Kondo lattice—or the related periodic Anderson model—agree in that the conduction electron bandwidth retains its original width of $2zt$ (with z the number of nearest neighbors); see, for example, Fig. 1 in Ref. [40], Fig. 3 in Ref. [19], or Fig. 4 in Ref. [28]. Any "correlation narrowing" of the conduction band thus obviously is unphysical. Moreover, as was discussed above, the bond Fermion theory without any constraint does reproduce the correct limiting value of the ground-state energy for $J/t \to 0$. This favorable property is lost if any renormalization of the hopping integrals is introduced. The best procedure therefore probably is to accept the inaccuracy and simply relax the constraint without further correction.

VI. CONCLUSION

In summary we have presented a theory for the ground state and single-particle spectrum of the Kondo lattice based on bond fermions. Thereby the constraint of having precisely one f electron per unit cell is fulfilled exactly; instead we are relaxing the hard-core constraint on the bond fermions which, however, turns out to be reasonably justified as the probability for violation of the constraint is low for not too small values of J/t. While being of comparable simplicity as the mean-field theory, the bond fermion theory gives results which differ significantly from the mean-field theory. Rather, the theory reproduces qualitatively a number of results obtained previously only by numerical methods. In particular we find two different antiferromagnetic phases: the first one with a small ordered moment and antiferromagnetically folded "heavy" bands where the localized electrons do contribute to the Fermi surface volume, and the second one with a larger ordered moment and a Fermi surface which corresponds to the back-folded Fermi surface of the conduction electrons alone and relatively light bands at the Fermi surface. Qualitatively the resulting phase diagram is quite consistent with experiments on $CeRhIn_5$. While in the present manuscript we have studied only simple two-sublattice Néel order the generalization to more complicated magnetic structures is self-evident.

[1] H. v. Löhneysen, A. Rosch, M. Vojta, and P. Wölfle, Rev. Mod. Phys. **79**, 1015 (2007).
[2] J. R. Schrieffer and P. A. Wolff, Phys. Rev. **149**, 491 (1966).
[3] S. Doniach, Physica B **91**, 231 (1977).
[4] A. Yoshimori and A. Sakurai, Prog. Theor. Phys. Supp. **46**, 162 (1970).
[5] C. Lacroix and M. Cyrot, Phys. Rev. B **20**, 1969 (1979).
[6] C. Lacroix, J. Magn. Magn. Mater. **100**, 90 (1991).
[7] G.-M. Zhang and L. Yu, Phys. Rev. B **62**, 76 (2000).
[8] T. Senthil, M. Vojta, and S. Sachdev, Phys. Rev. B **69**, 035111 (2004).
[9] G.-M. Zhang, Y.-H. Su, and L. Yu, Phys. Rev. B **83**, 033102 (2011).
[10] J. Nilsson, Phys. Rev. B **83**, 235103 (2011).
[11] M. Z. Asadzadeh, F. Becca, and M. Fabrizio, Phys. Rev. B **87**, 205144 (2013).
[12] S. J. Yamamoto and Q. Si, Phys. Rev. Lett. **99**, 016401 (2007).
[13] Q. Si, J. H. Pixley, E. Nica, S. J. Yamamoto, P. Goswami, R. Yu, and S. Kirchner, J. Phys. Soc. Jpn. **83**, 061005 (2014).
[14] M. Vojta, Phys. Rev. B **78**, 125109 (2008).
[15] E. Abrahams, J. Schmalian, and P. Wölfle, Phys. Rev. B **90**, 045105 (2014).
[16] G. Lonzarich, D. Pines, and Y. F. Yang, arXiv:1601.06050.
[17] S. Sachdev and R. N. Bhatt, Phys. Rev. B **41**, 9323 (1990).
[18] S. Gopalan, T. M. Rice, and M. Sigrist, Phys. Rev. B **49**, 8901 (1994).
[19] R. Eder, O. Stoica, and G. A. Sawatzky, Phys. Rev. B. **55**, R6109 (1997); R. Eder, O. Rogojanu, and G. A. Sawatzky, *ibid.* **58**, 7599 (1998).
[20] C. Jurecka and W. Brenig, Phys. Rev. B **64**, 092406 (2001).
[21] C. C. Yu and S. R. White, Phys. Rev. Lett. **71**, 3866 (1993). (The DMRG data for the ground-state energy are not published in this reference but seem to be given only in Ref. [22].)
[22] Z.-P. Shi, R. R. P. Singh, M. P. Gelfand, and Z. Wang, Phys. Rev. B **51**, 15630(R) (1995).
[23] F. F. Assaad, Phys. Rev. Lett. **83**, 796 (1999).
[24] R. Peters and T. Pruschke, Phys. Rev. B **76**, 245101 (2007).
[25] L. C. Martin, M. Bercx, and F. F. Assaad, Phys. Rev. B **82**, 245105 (2010).
[26] H. Watanabe and M. Ogata, Phys. Rev. Lett. **99**, 136401 (2007).
[27] N. Lanata, P. Barone, and M. Fabrizio, Phys. Rev. B **78**, 155127 (2008).
[28] L. C. Martin and F. F. Assaad, Phys. Rev. Lett. **101**, 066404 (2008).
[29] K. Kubo, J. Phys. Soc. Jpn. **84**, 094702 (2015).
[30] H. Shishido, R. Settai, D. Aoki, S. Ikeda, H. Nakawaki, N. Nakamura, T. Iizuka, Y. Inada, K. Sugiyama, T. Takeuchi, and K. Kin, J. Phys. Soc. Jpn. **71**, 162 (2002).
[31] S. K. Goh, J. Paglione, M. Sutherland, E. C. T. OFarrell, C. Bergemann, T. A. Sayles, and M. B. Maple, Phys. Rev. Lett. **101**, 056402 (2008).
[32] M. Yokoyama, H. Amitsuka, K. Matsuda, A. Gawase, N. Oyama, I. Kawasaki, K. Tenya, and H. Yoshizawa, J. Phys. Soc. Jpn. **75**, 103703 (2006).
[33] S. Ohira-Kawamura, H. Shishido, A. Yoshida, R. Okazaki, H. Kawano-Furukawa, T. Shibauchi, H. Harima, and Y. Matsuda, Phys. Rev. B **76**, 132507 (2007).
[34] S. Raymond, G. Knebel, D. Aoki, and J. Flouquet, Phys. Rev. B **77**, 172502 (2008).
[35] H. Shishido, R. Settai, H. Harima, and Y. Onuki, J. Phys. Soc. Jpn. **74**, 1103 (2005).
[36] R. Eder, Y. Ohta, and S. Maekawa, Phys. Rev. B **51**, 3265 (1995).
[37] S. Araki, R. Settai, T. C. Kobayashi, H. Harima, and Y. Onuki, Phys. Rev. B **64**, 224417 (2001).
[38] A. Hamann, O. Stockert, V. Fritsch, K. Grube, A. Schneidewind, and H. v. Löhneysen, Phys. Rev. Lett. **110**, 096404 (2013).
[39] P. W. Anderson, Phys. Rev. **86**, 694 (1952).
[40] K. Tsutsui, Y. Ohta, R. Eder, S. Maekawa, E. Dagotto, and J. Riera, Phys. Rev. Lett. **76**, 279 (1996).